MECSOL 2022 - Proceedings of the 8th International Symposium on Solid Mechanics
D. Bourdon, C.A. Souto and R.C. Reis, Campinas SP, Brazil, October 17th to 19th, 2022

Dynamic Evaluation of a Turbopump Rotor Supported by Magnetic Bearings

Daniel Bourdon [1], Carlos d'Andrade Souto [1], and Ronaldo Chaves Reis [1]

[1] Institute of Aeronautics and Space (IAE), São José dos Campos, SP, Brazil

Abstract: The development of a turbopump for liquid propellant rocket engines at the Institute of Aeronautics and Space (IAE) started in 2013 in the context of the L75 Project under the support of the Brazilian Space Agency (AEB). This development includes the design, manufacturing and testing of the turbopump components and assemblies for application in the L75 Rocket Engine. Due to its high rotational speed and interaction with high pressure fluids, the turbopump rotor dynamics is a crucial point for investigation. The vibration induced by the fluid flow in the pumps and the supersonic gas flow in the turbine can overload the bearings and is, usually, the main cause of turbopump failures. Ball bearings are commonly used for turbopump applications due to its high stiffness and accuracy, even though its low damping, fixed stiffness and the need of lubrication fluids motivated the development of innovative alternatives for stably supporting the turbopump rotor. Considering the moving parts are not in contact and so there is no need of lubrication, magnetic bearings have been considered as an alternative to high-speed rotors. This work evaluates the dynamic performance of the L75 engine turbopump rotor prototype radially supported by magnetic bearings. A numerical model is carried out considering the rotor as a rigid structure with a central disc magnetically supported by the shaft ends and driven by a specially designed control system. The magnetic interaction between the magnetic fields and the rotor movement is also considered. Time response graphics and performance index are presented in order to evaluate the capability of the magnetic bearings to dynamically stabilize the turbopump rotor.

Keywords: Turbopump, Rotor dynamics, Magnetic Bearing, Control System.

INTRODUCTION

In partnership with the German Space Agency (DLR) and with the financial support of the Brazilian Space Agency (AEB), the Institute of Aeronautics and Space (IAE) has been developing a liquid propellant rocket engine entitled Project L75 since 2013. The L75 rocket engine is designed for the last stage application of satellite launch vehicles, has a thrust of 75 kN and uses renewable and ecologically green propellants: ethanol and liquid oxygen

L75 Engine Turbopoump

The turbopump is responsible for pressurizing and injecting the propellants into the combustion chamber. It consists of two centrifugal pumps and a supersonic turbine mounted on the same shaft. The turbopump shaft is supported by angular contact ball bearings, which support the radial and axial loads from the pump impellers and the turbine, which provides the pumps with 400 kW power at 24,000 rpm. A schematic of the L75 turbopump is shown in the Fig. 1.

Tests of pump prototypes were carried out in 2017 and showed high vibration levels in the bearings at speeds above 18,000 rpm, compromising the dynamic stability and reliability of the rotating assembly. Although vibration is mainly caused by the interaction of the fluid with the pump blades, adjusting the stiffness and damping of the bearings becomes essential to avoid resonance phenomena between the fluid and the rotating assembly in the different operating conditions of the rocket motor (Almeida,2014).

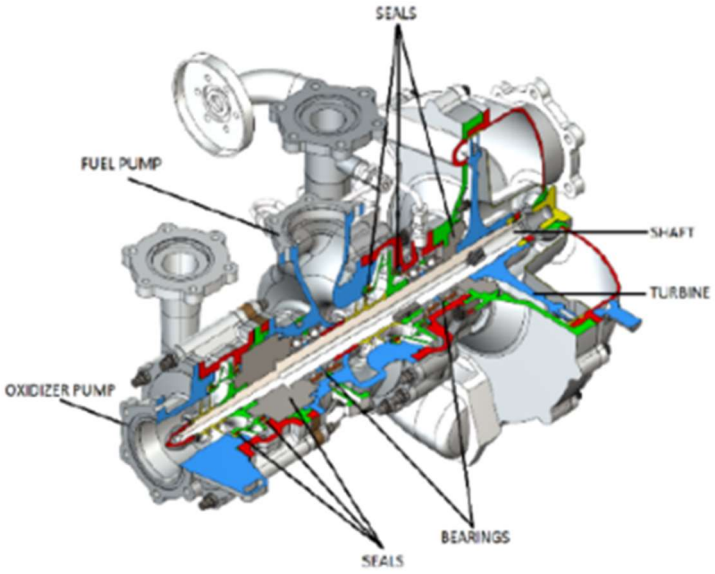

Figure 1 - Sectional diagram of the L75 engine turbopump.

Magnetic Bearings

Widely used in industry, magnetic bearings are systems for supporting rotating rotors that use magnetic levitation. It can be defined by a stable condition of an object without any mechanical contact with the external environment, where its weight is supported only by magnetic forces. The condition of the object must remain stable even subjected to reasonable external disturbances, in all degrees of freedom.

Basically, there are two types of magnetic bearings: the active ones, whose levitation is maintained by means of a control system that processes and amplifies the sensor signal; and the passive ones, whose levitation is maintained by permanent magnets, without a control loop, using magnetic repulsion. The most used type is the active magnetic bearings due to its adaptability to the equipment operating conditions and, therefore, this is the type used in this study.

A magnetic bearing has several advantages over conventional bearings, such as reducing vibration, improving robustness and increasing performance, mainly in high-speed applications (Antila,1998). With no contact between rotating and stationary parts, there is no mechanical wear, eliminating the need for lubrication and frequent maintenance, as well as increasing service life. The operation is monitored electronically, providing maintenance before any risk of damaging the main system. Generally, magnetic bearings are used in systems that require high rotational speed and high performance, in equipment operating in aseptic or vacuum environments, in precision systems and in systems that require no contact or low vibration (Youncef-Toumi,1992). Examples of application are: aseptic fluid pumps, vacuum pumps (turbomolecular), industrial turbines, mechanical batteries, gyroscopes, satellites and space stations, as well as vibration reduction systems for industrial equipment. Some applications are shown in the Fig. 2.

Figure 2 - Applications of magnetic bearings in industry.

MAGNETIC BEARINGS APPLIED TO THE L75 ENGINE TURBOPUMP

Considering the high angular speed (24,000 rpm), the operation mainly in space environment (vacuum), the flow of reactive fluids (liquid oxygen, high temperature gas) and high-frequency cyclic loads (turbulent fluid flow), the magnetic bearings are a great alternative to mitigate the risk of failure in the L75 engine turbopump.

During the tests of the turbopump components, carried out in 2016-17 at the IAE, it was observed the occurrence of intense vibration in the bearings, probably related to phenomena of cavitation and fluid recirculation, in the pumps, and to shock waves in the vanes in the turbine. The occurrence of these loads is inherent to the turbopump operation and can hardly be avoided.

The turbopump bearing configuration (2 pairs of angular contact ball bearings) is a very reasonable option, as it is widely used in high-speed machine tools (mills and grinders) and presents high stiffness. However, due to the nature of their construction, the ball bearings do not have useful damping and their stiffness is highly dependent on mounting and operating conditions, such as angular speed and the direction of loads. There are also effects on stiffness related to differences in thermal expansion of the bearing components, taking the system at risk of vibration failure.

Therefore, an active magnetic bearing, with the possibility of adjusting the dynamic properties during operation, becomes fundamental for the development of a reliable and efficient turbopump. Despite being slightly heavier, magnetic bearings are considered a great option for this application.

As it was never developed at IAE, it is necessary to build a prototype of the magnetic bearing to verify the feasibility of the project, the methods of production and the performance of an active control system. This prototype consists of a rotating shaft driven by an electric motor and supported by magnetic bearings controlled by a programmable electronic system. A schematic of this prototype is presented in the Fig. 3.

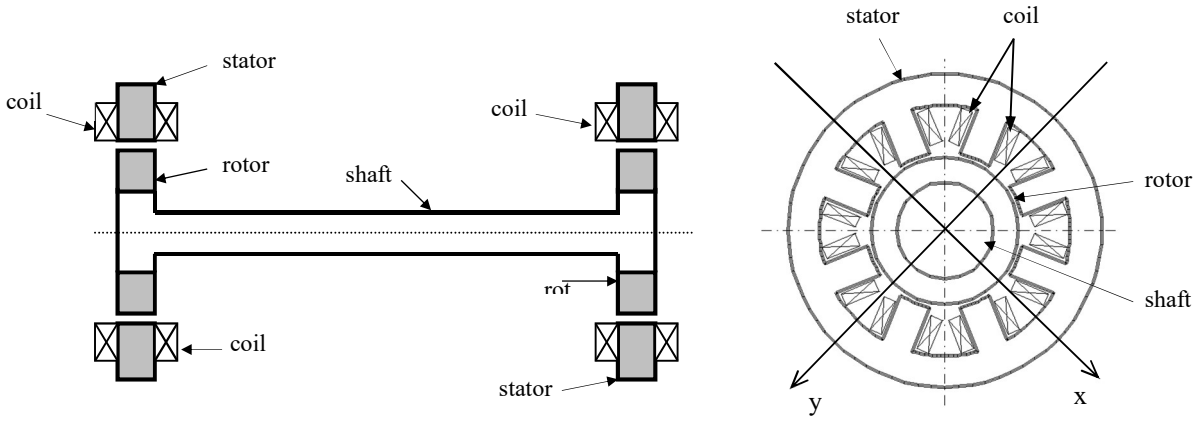

Figure 3 - Scheme of the dynamic prototype of the turbopump rotor (front and lateral views).

The purpose of this study is, therefore, to elaborate a mathematical model describing the dynamics of a rotor levitated by magnetic bearings, stabilized by a closed-loop controller, and subjected to constant and time-dependent external forces.

The design of the bearing rotor and the electromagnet was carried out by the team responsible for the prototype design and it is beyond the scope of this work. Therefore, some characteristics relevant to the dynamics of the system and the limitations imposed by the equipment available in the test bench was considered, resulting on the magnet geometry presented in the Figure 3 (lateral view), the voltage limited to 20V and the current to 5A in each electromagnet. The acquisition system has 16 channels and operates at an acquisition rate of 10 kHz. These specifications define the project and, consequently, the dimensions of the electromagnets and rotors of the dynamic prototype, as shown in Table 1.

Table 1. Design parameters of the magnetic bearing prototype.

Parameter	Symbol	Value	Unity
Rotor mass	m	3,0	kg
Electromagnet gap	h	$5{,}75.10^{-4}$	m
Shaft length	L_e	0,3	m
Initial current	I_o	0,1	A
Electromagnet resistance	R_e	5,0	ohm
Number of coils	N_e	182	-

Parameter	Symbol	Value	Unity
Transversal area of magnetic flux	S_f	$3{,}13.10^{-4}$	m^2
Coil tilt (with *x* axis)	ϕ_b	π /8	rad
Magnetic loss coefficient	K_f	1,05	-
magnetic permeability of air	μ_o	$4.10^{-7}.\pi$	-

MATHEMATICAL MODEL OF THE PROTOTYPE ROTORDYNAMICS

The dynamic model of the prototype was developed in two stages: a unidimensional magnetic bearing model (1 GL) and a tridimensional rotating rigid rotor model (4 GL).

Magnetic Bearing Model

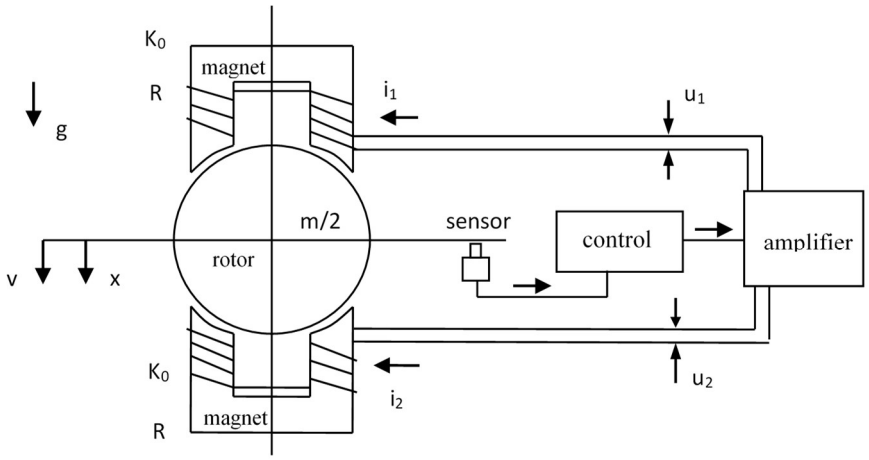

Figure 4 - Dynamic scheme of the magnetic bearing.

The magnetic bearing model is composed by a mass, representing the bearing rotor, two electrical circuits, representing the power supply to the electromagnets, and two magnetic circuits, representing the opposed action of the electromagnets. The rotor motion, in this model, occurs in only one direction, therefore, it has only 1 degree of freedom.

The electromagnet circuit can be represented as a resistor and an inductor connected in series, as shown in Fig. 5.

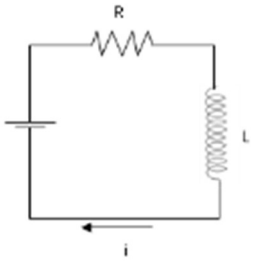

Figure 5 - Electromagnet electrical scheme.

Thus, the equation of the electrical circuit can be represented by:

$$V = L \cdot \frac{di}{dt} + R.i \tag{1}$$

where V is voltage, L is inductance, R is electrical resistance, i is electrical current and t is time. The strength of the magnetic field in the electromagnet is defined by:

$$H_f = \frac{\emptyset}{\mu_o \cdot S_f} \tag{2}$$

where $\emptyset$ is the magnetic flux, μ_o is the magnetic permeability of air and S_f is the cross-sectional area of the magnetic flux. Therefore, the magnetic force, which is an effect of the difference in magnetic permeability between the air and the electromagnet material (due to the presence of a gap between the electromagnet and the rotor), is defined as:

$$F_{mag} = \frac{K_0}{2} \cdot \frac{(I+i)^2}{(h+x)^2} \tag{3}$$

where K_0 is the electromagnet constant, I is the initial electric current (constant), i is the electric current in the circuit, h is the initial gap between the electromagnet and the rotor, and x is the rotor displacement. It can be seen, from the magnetic force equation, that it is inversely proportional to the square of the rotor position, demonstrating a very non-linear characteristic of the electromagnet dynamics.

The constant of the electromagnet, according to its design, is defined by

$$K_0 = \frac{2.\mu_o.K_f.S_f.N^2}{\cos\beta} \tag{4}$$

where K_f is the ratio between the total magnetic flux and the useful flux in the electromagnet, N is the number of turns in the coil, and β is the angle of the magnetic flux in the gap with respect to the electromagnet's axis of symmetry.

In this way, the inductance is defined by:

$$L = \frac{2.N.\emptyset}{(I+i)} = \frac{K_o}{(x+h)} \tag{5}$$

The dynamic model of the magnetic bearing was defined using Lagrange's equations. Choosing x (axis position), q_1 and q_2 (electrical charges on the turns) as the generalized coordinates, we have:

$$\begin{cases} \frac{d}{dt}\left(\frac{\partial(T-U)}{\partial \dot{x}}\right) - \frac{\partial(T-U)}{\partial x} + \frac{\partial D}{\partial \dot{x}} = Q_x \\ \frac{d}{dt}\left(\frac{\partial(T-U)}{\partial \dot{q}_1}\right) - \frac{\partial(T-U)}{\partial q_1} + \frac{\partial D}{\partial \dot{q}_1} = Q_{q_1} \\ \frac{d}{dt}\left(\frac{\partial(T-U)}{\partial \dot{q}_2}\right) - \frac{\partial(T-U)}{\partial q_2} + \frac{\partial D}{\partial \dot{q}_2} = Q_{q_2} \end{cases} \tag{6}$$

Defining T as kinetic energy, U as potential, and D dissipated energy, then:

$$T = \frac{1}{2} m \cdot \dot{x}^2 + \frac{1}{2} \cdot L_1 \cdot \dot{q}_2^2 + \frac{1}{2} \cdot L_2 \dot{q}_2^2 \tag{7}$$

$$D = \frac{1}{2} \cdot R_1 \cdot \dot{q}_1^2 + \frac{1}{2} \cdot R_2 \cdot \dot{q}_2^2 \tag{8}$$

Doing:

$$Q_x = F_c \tag{9a}$$
$$Q_{q_1} = U_1 + u_1 \tag{9b}$$
$$\dot{q}_1 = i_1 + I_1 \tag{9c}$$
$$\dot{q}_2 = i_2 + I_2 \tag{9d}$$
$$L_1 = \frac{K_O}{(h+x)} \tag{9e}$$
$$L_2 = \frac{K_O}{(h-x)} \tag{9f}$$
$$\dot{x} = v \tag{9g}$$

where U and I are initial values of voltage and current in electromagnets 1 and 2, u is the voltage applied to circuits 1 and 2, and E_e is an external force applied to the rotor (loads and weight). By applying Lagrange's equations on the expressions of kinetic and potential energies (eqs. 7 and 8) combined with equations (9a-9g) the magnetic bearing dynamics can then described by the following equations:

$$\begin{cases} m\dot{v} + \frac{1}{2}K_o \cdot \frac{(I_1 + i_1)^2}{(h+x)^2} - \frac{1}{2}K_0 \cdot \frac{(I_2 + i_2)^2}{(h-x)^2} = F_e \\ \left[\frac{K_O}{(h+x)}\right]\frac{di_1}{dt} - K_O \cdot v \cdot \frac{(I_1 + i_1)}{(h+x)^2} + R_1 \cdot (I_1 + i_1) = U_1 + u_1 \\ \left[\frac{K_O}{(h-x)}\right]\frac{di_2}{dt} + K_O \cdot v \cdot \frac{(I_2 + i_2)}{(h-x)^2} + R_2 \cdot (I_2 + i_2) = U_2 + u_2 \end{cases} \quad (10)$$

By including eq (9g) we can transform the above system into a 1st order system of differential equations:

$$\begin{cases} \dot{x} = v \\ \dot{v} = -\frac{K_0 \cdot (I_1 + i_1)^2}{2.m.(h+x)^2} + \frac{K_o \cdot (I_2 + i_2)^2}{2.m.(h-x)^2} + \frac{F_e}{m} \\ \frac{di_1}{dt} = \left[\frac{(h+x)}{K_0}\right] \cdot \left[U_1 + u_1 + \left(\frac{K_0 \cdot v}{(h+x)^2} - R_1\right) \cdot (I_1 + i_1)\right] \\ \frac{di_2}{dt} = \left[\frac{(h-x)}{K_0}\right] \cdot \left[U_2 + u_2 + \left(\frac{-K_0 \cdot v}{(h-x)^2} - R_2\right) \cdot (I_2 + i_2)\right] \end{cases} \quad (11)$$

Considering that the bearing control system will act on opposing electromagnets in an equivalent way, that is, making the control variable $u_1 = -u_2$, we can simplify the bearing system of equations by eliminating an equation. Then, representing the system in a matrix form:

$$\begin{bmatrix} \dot{x}_1 \\ \dot{v}_1 \\ \frac{di_1}{dt} \end{bmatrix} = \begin{bmatrix} v_1 \\ -\frac{K_O(I_0 + i_1)^2}{2.m(h+x_1)^2} + \frac{K_O(I_0 - i_1)^2}{2.m(h-x_1)^2} \\ \frac{U_1}{K_O}(h+x_1) + \frac{v_1.(I_0 + i_1)}{(h+x_1)} - \frac{R_1}{K_O}(h+x_1)(I_0 + i_1) \end{bmatrix} + \begin{bmatrix} 0 \\ 0 \\ \frac{(h+x_1)}{K_O} \end{bmatrix} u_1 \quad (12)$$

where $I_0 = I_1 = I_2$ and $x_1 = x$ is the displacement of the rotor in one direction.

Magnetic bearing control system

The control system was designed by State Feedback based on the linearized magnetic bearing system.

Expanding the system of equations for the bearing in a Taylor series around the operating point and neglecting the higher order terms, we have:

$$\begin{bmatrix} \dot{x}_1 \\ \dot{v}_1 \\ \frac{di_1}{dt} \end{bmatrix} = \begin{bmatrix} v_1 \\ -\frac{2K_0.I_0}{mh^2}i_1 + \frac{2K_0 I_0^2}{mh^3}x_1 \\ \frac{I_0}{h}v_1 - \frac{R.h}{K_0}i_1 \end{bmatrix} + \begin{bmatrix} 0 \\ 0 \\ \frac{h}{K_0} \end{bmatrix} u_1 \quad (13)$$

Representing eq.(13) in state space ($\dot{\boldsymbol{x}} = \boldsymbol{Ax} + \boldsymbol{Bu}$) and simplifying:

$$\dot{\boldsymbol{x}}_1 = \begin{bmatrix} 0 & 1 & 0 \\ \frac{k_x}{m} & 0 & -\frac{k_i}{m} \\ 0 & \frac{k_x}{k_i} & -\frac{R}{L_0} \end{bmatrix} \boldsymbol{x}_1 + \begin{bmatrix} 0 \\ 0 \\ \frac{1}{L_0} \end{bmatrix} u_1 \quad (14)$$

where:

$$k_x = \frac{2K_0.I_0^2}{h^3} \quad (15)$$

$$k_i = \frac{2K_0.I_0}{h^2}$$

$$L_0 = \frac{K_0}{h}$$

The map of the location of the poles and zeros of this system with the state variable x as output is presented in Figure 6. We can deduce that the system is unstable in the vicinity of the equilibrium point, therefore the performance of a control system is fundamental for the rotor stability.

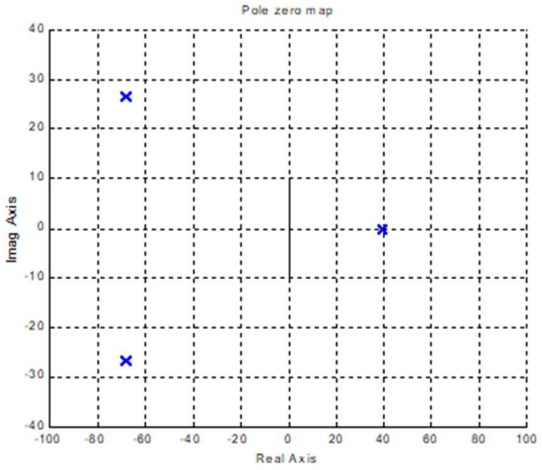

Figure 6. Position of the poles and zeros of the linearized magnetic bearing.

The state feedback control function, considering that the system is controllable, is defined by Ogata (1990):

$$u = -\boldsymbol{K}.\boldsymbol{x} \tag{16}$$

where:

$$\mathbf{x} = [w\ x\ v\ i]^T \quad \text{and} \quad \boldsymbol{K} = [K_1 \quad K_2 \quad K_3 \quad K_4] \tag{16a,16b}$$

Note the inclusion of the state variable *w* representing the integral of the variable x, for control purposes.

The state feedback matrix *K* is defined by the Ackermann formula (Ogata,1990):

$$\mathbf{K} = [0 \quad 0 \quad 0 \quad 1].[\mathbf{B} \quad \mathbf{AB} \quad \mathbf{A^2B} \quad \mathbf{A^3B}]^{-1}.\varphi(\mathbf{A}) \tag{17}$$

where $\varphi(\mathrm{A})$ is defined by the Cayley-Hamilton theorem, where A satisfies the characteristic equation itself:

$$\boldsymbol{\varphi}(\mathbf{A}) = \mathbf{A}^4 + a_1.\mathbf{A}^3 + a_2.\mathbf{A}^2 + a_3.\mathbf{A} + a_4.\mathbf{I} \tag{18}$$

The indices a_i of this equation, in turn, are determined considering the desired response of the system, which, in this case, was defined with an over-signal $\boldsymbol{M_p}$ of 10% and an accommodation time $\boldsymbol{t_s}$ of 0.1 s.

The control gains, defined by the state feedback matrix K, are shown in Table 2.

Tabela 2. Control system gains.

Parameter	Symbol	Value	unity
Integral (x)	K_1	1,22.107	V/m.s
Proportional (x)	K_2	2,59.105	V/m
Derivative (x)	K_3	3,21.103	V.s/m
Proportional (i)	K_4	-81,9	V/A

In this way, the matrix representation of the magnetic bearing dynamics with control system is:

$$\begin{bmatrix} \dot{w}_1 \\ \dot{x}_1 \\ \dot{v}_1 \\ \dfrac{di_1}{dt} \end{bmatrix} = \begin{bmatrix} x_1 \\ v_1 \\ -\dfrac{K_O(I_0+i_1)^2}{2.m(h+x_1)^2} + \dfrac{K_O(I_0-i_1)^2}{2.m(h-x_1)^2} \\ \dfrac{U_1}{K_O}(h+x_1) + \dfrac{v_1.(I_0+i_1)}{(h+x_1)} - \dfrac{R_1}{K_O}(h+x_1)(I_0+i_1) \end{bmatrix} + \begin{bmatrix} 0 \\ 0 \\ 0 \\ \dfrac{(h+x_1)}{K_O} \end{bmatrix} [K_1 \quad K_2 \quad K_3 \quad K_4] \begin{bmatrix} s_1 \\ x_1 \\ v_1 \\ i_1 \end{bmatrix} \tag{19}$$

The position of the poles and zeros of the system with state feedback control is shown in Fig. 7.

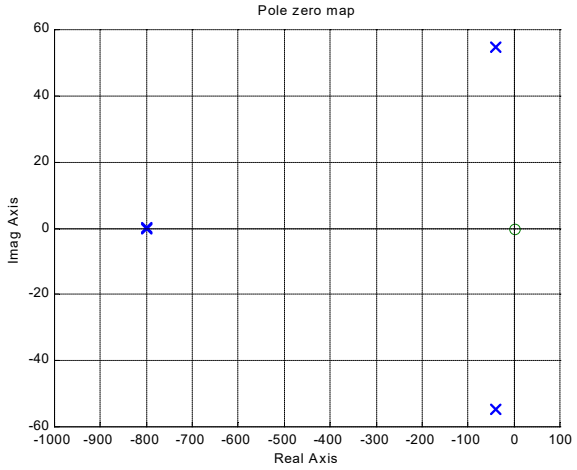

Figure 7. Position of bearing poles and zeros with control system.

Rotor model

The dynamic equations were developed considering the acting forces F in the free rigid body rotor, the position of the shaft center of mass along the x and y directions, considering four degrees of freedom, as shown in Figure 8. In this paper it is considered translation displacements of the shaft center of mass respectively in the x and y directions (x_c) and (y_c) and angles of rotation about y axis (θ) and about x axis (φ). By geometric considerations these angles are assumed to be small. The gyroscopic effect due to shaft spin (ω) is included in the model.

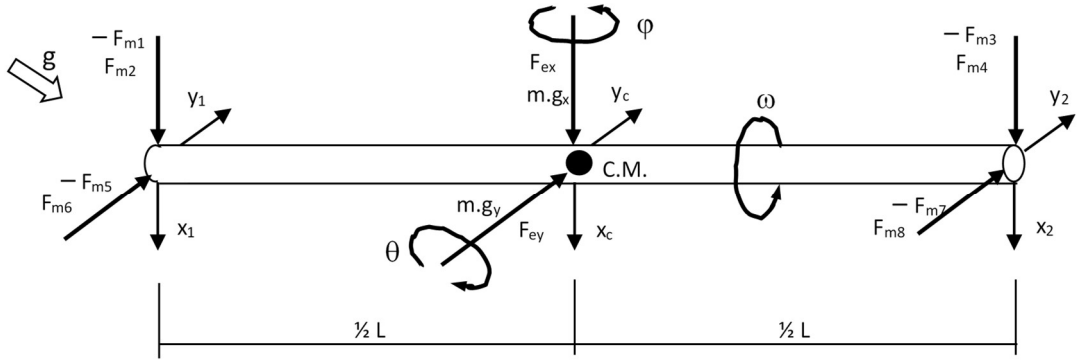

Figure 8. Dynamic representation of the rotating rotor.

The dynamic model of the rotating rotor was defined using the Newton-Euler equations for rigid bodies in three-dimensional motion. As the reference axes coincide with the principal axes of inertia and the speed of rotation around the axial axis is constant, the equations of the dynamics of the rotating rotor becomes as:

$$\begin{cases} m.\ddot{x}_c = \sum F_{mx} + F_{ex} + mg_x & (20a) \\ m.\ddot{y}_c = \sum F_{my} + F_{ey} + mg_y & (20b) \\ J_r.\ddot{\theta} = \frac{L}{2}\sum F_{m\theta} - J_a.\omega.\dot{\varphi} & (20c) \\ J_r.\ddot{\varphi} = \frac{L}{2}\sum F_{m\phi} + J_a.\omega.\dot{\theta} & (20d) \end{cases}$$

where m is the rotor mass, x_c and y_c are the displacements of the CG with respect to the x and y axes, respectively, φ and θ are the angular displacements with respect to the x and y axes, respectively, J_a and J_r are the moments of inertia of the rotating rotor with respect to the axial (z) and radial (x or y) axes, respectively, ω is the rotation speed in the axial (z) direction (constant), F_{mi} (i=*1,2...8*) are the sum of the magnetic bearing reactions and F_{ex} and F_{ey} are the external forces in the x and y directions applied to the CG. The reactions in the bearings are:

$$\begin{cases} \sum F_{mx} = -F_{m1} + F_{m2} - F_{m3} + F_{m4} & (21a) \\ \sum F_{my} = -F_{m5} + F_{m6} - F_{m7} + F_{m8} & (21b) \end{cases}$$

$$\begin{cases} \sum F_{m\theta} = F_{m1} - F_{m2} - F_{m3} + F_{m4} & (21c) \\ \sum F_{m\varphi} = F_{m5} - F_{m6} - F_{m7} + F_{m8} & (21d) \end{cases}$$

In this study we assume that the reference system is non-inertial and, therefore, the effects of the displacement of the CG contained in the *xy* plane are defined by the centrifugal force (inertial force). Therefore, the external forces are composed of the centrifugal force and the operating loads (f_o), both applied to the CG of the rotor, as well as:

$$F_{ex} = m \cdot \omega^2 \cdot R_e \,.\, sen(\omega t) + f_{ox} \quad (22a)$$

$$F_{ey} = m \cdot \omega^2 \cdot R_e . cos(\omega t) + f_{oy} \quad (22b)$$

where R_e is the distance between the geometric center and the rotor mass center, whose maximum value is specified by the ISO 1941 standard. In the case of the L75 engine turbopump, this value is 2 μm. The values of the rotating rotor parameters are shown in Table 3.

Table 3. Rotor model parameters.

Parameter	Symbol	Value	unity
Rotor mass	m	3,0	kg
Radial moment of inertia	J_r	0,141	kg.m^2
Axial moment of inertia	J_a	3,08.10^{-3}	kg.m^2
Rotation speed	ω	20.000	rpm
CG displacement	R_e	2.10^{-6}	m

However, the bearing reactions (F_{mi}) are part of the bearing dynamic equations defined above. To define the dynamics of the rotor completely, we must merge the equations that define the dynamics of the bearings with the rigid body equations of the rotor. Initially, we define the relationship between the magnetic bearing variables and the rotor ones:

$$x_1 = x_c + \frac{L}{2}\theta \quad (23a)$$

$$x_2 = x_c - \frac{L}{2}\theta \quad (23b)$$

$$y_1 = y_c + \frac{L}{2}\varphi \quad (23c)$$

$$y_2 = y_c - \frac{L}{2}\varphi \quad (23d)$$

Finally, by manipulating the rotor dynamic equations and combining it with the magnetic bearing model, the resulting 1st order system variables will be:

$$\begin{bmatrix} x_1 \\ x_2 \\ \vdots \\ x_{16} \end{bmatrix} = \left[\int x_c \quad x_c \quad \dot{x}_c \quad \int y_c \quad y_c \quad \dot{y}_c \quad \int \theta_c \quad \theta_c \quad \dot{\theta}_c \quad \int \varphi_c \quad \varphi_c \quad \dot{\varphi}_c \quad i_1 \quad i_2 \quad i_3 \quad i_4 \right]^T \quad (24)$$

and the resulting 1st order system will be defined by:

$$\begin{bmatrix}\dot{x}_1\\ \dot{x}_2\\ \dot{x}_3\\ \dot{x}_4\\ \dot{x}_5\\ \dot{x}_6\\ \dot{x}_7\\ \dot{x}_8\\ \dot{x}_9\\ \dot{x}_{10}\\ \dot{x}_{11}\\ \dot{x}_{12}\\ \dot{x}_{13}\\ \dot{x}_{14}\\ \dot{x}_{15}\\ \dot{x}_{16}\end{bmatrix} = \begin{bmatrix} x_2 \\ x_3 \\ \frac{(-F_{m1}+F_{m2}-F_{m3}+F_{m4}+F_{ex})}{m} \\ x_5 \\ x_6 \\ \frac{(-F_{m5}+F_{m6}-F_{m7}+F_{m8}+F_{ex})}{m} \\ x_8 \\ x_9 \\ \frac{L}{2J_r}(F_{m1}-F_{m2}-F_{m3}+F_{m4}) - \frac{J_a.\omega.x_{12}}{J_r} \\ x_{11} \\ x_{12} \\ \frac{L}{2J_r}(F_{m5}-F_{m6}-F_{m7}+F_{m8}) + \frac{J_a.\omega.x_9}{J_r} \\ \left(h+x_2+\frac{L}{2}x_8\right)\left[\frac{U_1}{K_O}+\frac{v_1.(I_0+x_{13})}{\left(h+x_2+\frac{L}{2}x_8\right)^2}-\frac{R_1}{K_O}(I_0+x_{13})+\frac{(K_1x_1+K_2x_2+K_3x_3+K_4x_{13})}{K_O}\right] \\ \left(h+x_2-\frac{L}{2}x_8\right)\left[\frac{U_1}{K_O}+\frac{v_1.(I_0+x_{14})}{\left(h+x_2-\frac{L}{2}x_8\right)^2}-\frac{R_1}{K_O}(I_0+x_{14})+\frac{(K_1x_4+K_2x_5+K_3x_6+K_4x_{14})}{K_O}\right] \\ \left(h+x_5+\frac{L}{2}x_{11}\right)\left[\frac{U_1}{K_O}+\frac{v_1.(I_0+x_{15})}{\left(h+x_5+\frac{L}{2}x_{11}\right)^2}-\frac{R_1}{K_O}(I_0+x_{15})+\frac{(K_1x_7+K_2x_8+K_3x_9+K_4x_{15})}{K_O}\right] \\ \left(h+x_5-\frac{L}{2}x_{11}\right)\left[\frac{U_1}{K_O}+\frac{v_1.(I_0+x_{16})}{\left(h+x_5-\frac{L}{2}x_{11}\right)^2}-\frac{R_1}{K_O}(I_0+x_{16})+\frac{(K_1x_{10}+K_2x_{11}+K_3x_{12}+K_4x_{16})}{K_O}\right] \end{bmatrix} \quad (25)$$

where:

$$F_{m_1} = \frac{K_0}{2}\cdot\frac{(I_0+x_{13})^2}{\left(h+x_2+\frac{L}{2}x_8\right)^2}, \quad F_{m_2} = \frac{K_0}{2}\cdot\frac{(I_0-x_{13})^2}{\left(h-x_2-\frac{L}{2}x_8\right)^2} \quad (26a,b)$$

$$F_{m_3} = \frac{K_0}{2}\cdot\frac{(I_0+x_{14})^2}{\left(h+x_2-\frac{L}{2}x_8\right)^2}, \quad F_{m_4} = \frac{K_0}{2}\cdot\frac{(I_0-x_{14})^2}{\left(h-x_2+\frac{L}{2}x_8\right)^2} \quad (27a,b)$$

$$F_{m_5} = \frac{K_0}{2}\cdot\frac{(I_0+x_{15})^2}{\left(h+x_5+\frac{L}{2}x_{11}\right)^2}, \quad F_{m_6} = \frac{K_0}{2}\cdot\frac{(I_0-x_{15})^2}{\left(h-x_5-\frac{L}{2}x_{11}\right)^2} \quad (28a,b)$$

$$F_{m_7} = \frac{K_0}{2}\cdot\frac{(I_0+x_{16})^2}{\left(h+x_5-\frac{L}{2}x_{11}\right)^2}, \quad F_{m_8} = \frac{K_0}{2}\cdot\frac{(I_0-x_{16})^2}{\left(h-x_5+\frac{L}{2}x_{11}\right)^2} \quad (29a,b)$$

RESULTS OF NUMERICAL SIMULATIONS

The performance of the magnetic bearings, in relation to the dynamic stabilization of the rotating rotor, was evaluated through numerical simulation of the mathematical model developed in this study using a code developed in Python 3.7. The evaluation was performed based on time response of the system subjected to step input, impulse input and on external forces simulating unbalance and operating loads.

Considering that the step input at x_c or y_c cannot have a value greater than the gap (h) between the rotor and the electromagnet, the highest initial value with a stable response was simulated. Therefore, the simulation of the time response to the 0.1 mm step at x_c and the 0.02 m/s impulse at $\dot{y}_c$, in addition to the rotor CG trajectory, is shown in Fig. 9.

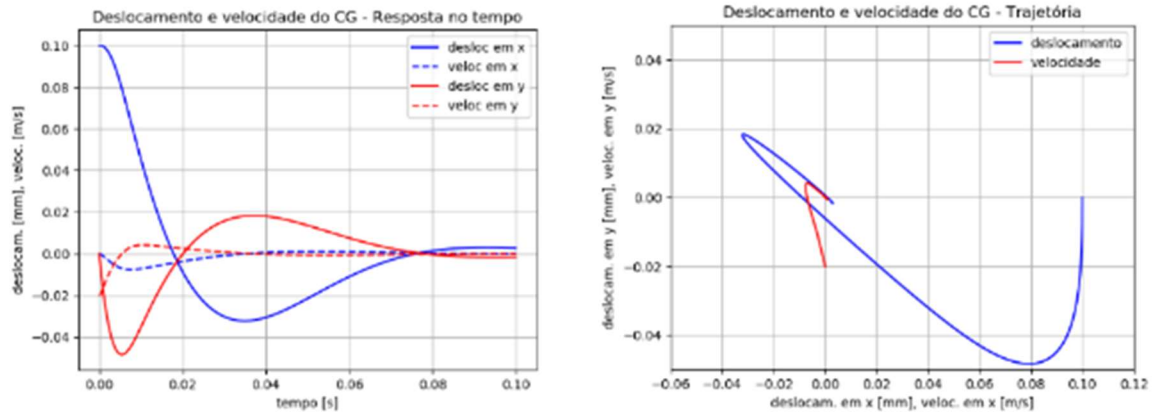

Figure 9. Step response at x_c and impulse response at y_c: CG time and trajectory response.

It can be observed that the system, naturally unstable, became stable by action of the control system, presenting an accommodation time as expected (0.1s), but the over-signal was slightly higher than expected (10%), probably due to the non-linear nature of the magnetic forces. The response becomes unstable for step and impulse values greater than the presented one.

Additionally, a step response simulation of 0.03 mrad in θ and impulse of 0.03 rad/s in $\dot{\varphi}$ was performed. The results of the time response and the GC trajectory are shown in Figure 10.

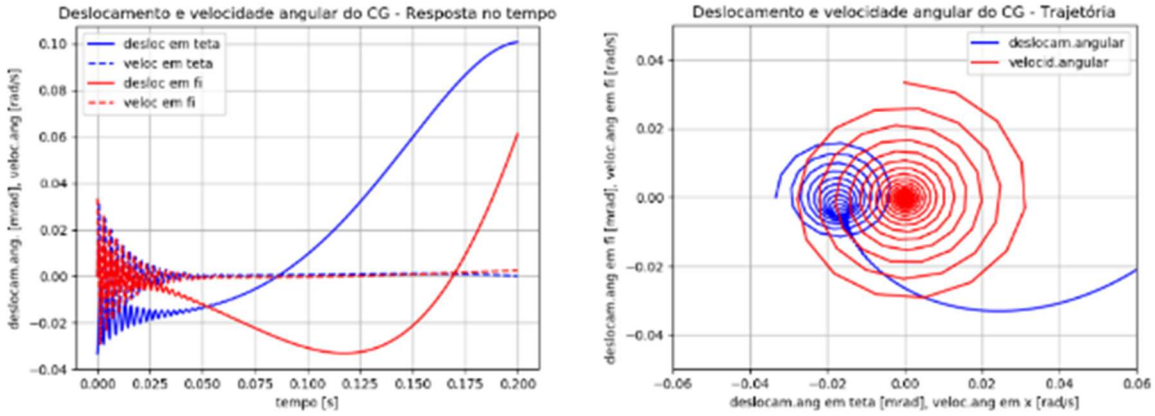

Figure 10. Step response in θ and impulse response in φ: time response and CG trajectory.

It can be seen that the system response is not stable for motion in angular directions. This is probably due to the rigid body dynamics of the rotor not being covered by the control system. It is noteworthy that the result is not different for smaller step and impulse values. The electrical current did not exceed 0.3 A in the cases presented above, so the power required to control the bearing was less than 0.5 W.

The response of the system subjected to the force due to the rotor CG displacement by 2 μm in the *xy* plane and the operating force of 10 N (constant) is shown in Figure 11. These conditions reasonably simulate the actual operating conditions of the rotor of the turbopump. The response remains stable.

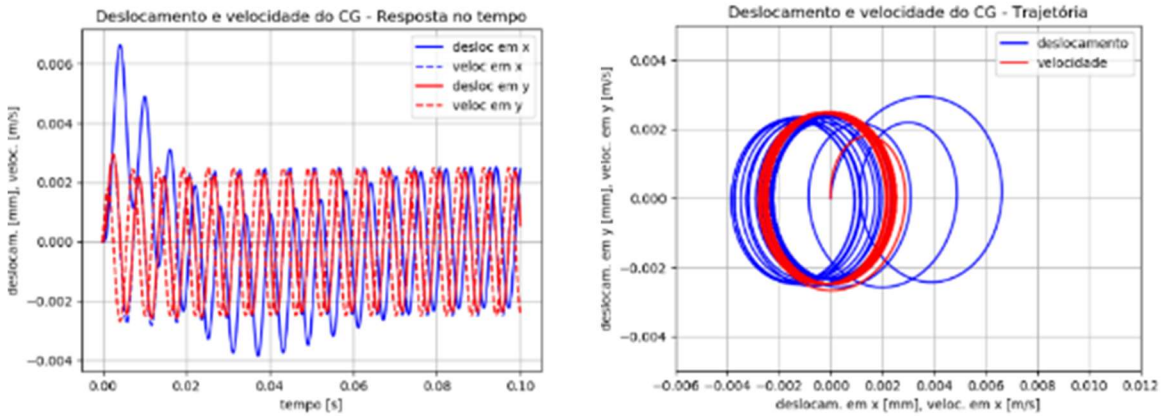

Figure 11. Rotor unbalance response: GC time and trajectory response.

The oscillation amplitude is not high (about 4 μm), but it can be noticed that the control is not fast enough to dampen the vibration. The maximum electrical current used by the control was 0.1 A (power of 0.05 W).

CONCLUSIONS

The mathematical model of the L75 engine turbopump rotating rotor prototype, developed in this study, showed to be very promising for the evaluation and development of magnetic bearing control systems. The translational and rotational movements of the rotor, as well as the inertia forces and the dynamics of the electromagnets, were satisfactorily reproduced by the simulation.

The control system chosen (state feedback) for the magnetic bearing showed satisfactory results for the stabilization of the rotor when subjected to translational movements, but it did not demonstrate stability when the rotor was subjected to rotation around the radial axis. (x,y). This is probably due to the design of the control system is not considering the rigid body dynamics of the rotor, considering it only as a mass point.

The dynamics of the magnetic bearings was modeled using Lagrange's equations, while the rigid body dynamics of the rotor was modeled using the Newton-Euler equations for three-dimensional general motions, considering the axes of rotation coincident with the principal axes of inertia and considering the displacement of the CG as an inertia force. The rotating rotor and magnetic bearing mathematical models were merged to describe the full dynamics of the turbopump rotating rotor prototype.

Despite meeting the needs of the simulation, the dynamic model of the rotor could be more realistic if it could consider the CG out of the geometric center and the dynamics of a flexible shaft, which would allow the simulation of the vibration modes of the shaft and the evaluation of the performance of the bearings and the control system under more realistic conditions. These changes is planned to be carried out in the future, as far as the construction and testing of a rotor supported by the magnetic bearings as presented here.

Additionally, other types of control systems, such as PID or non-linear controls, will be developed to evaluate the feasibility of the implementation of magnetic bearings in the L75 engine turbopump rotor.

Acknowledgements. The authors wish to thank AEB/IAE for supporting all activities performed in the frame of the L75 project. This study was financed in part by the Coordenação de Aperfeiçoamento de Pessoal de Nível Superior - Brasil (CAPES) - Finance Code 001.

REFERENCES

ALMEIDA, D.S. and PAGLIUCO, C.M.M, “Development Status of L75: A Brazilian Liquid Propellant Rocket Engine”, Journal of Aerospace Technology and Management, Vol.6, No 4, Oct.-Dec., 2014, pp.475-484.

ANTILA, M.; LANTTO, E. ; ARKKIO, A. Determination of Forces and Linearized Parameters of Radial Active Magnetic Bearings by Finite Element Technique. IEEE Transaction on Magnetics. Vol. 34, no 3. May, 1998.

BITTAR, A. Controle da Suspensão Eletromagnética do Protótipo de um Veículo. Tese apresentada à Escola Politécnica, USP. São Paulo, 1998.

BOLTON, W. Engenharia de Controle. Makron Books do Brasil Ed. Ltda. Trad.: Valceres Vieira Rocha e Silva, MsC. São Paulo, 1995.

BOURDON, D., ZINK, E.S., NEIAS Junior, V., KITSCHE, W., WAGNER, B. “Manufacturing and Examination of Impeller Prototypes for Rocket Propulsion Systems”, *to be published 66. DLRK*, 2017.

BUTNER, M. F., KELLER, R. B., Jr. „ Liquid rocket engine turbopump bearings - Space vehicle design criteria", Technical Report, NASA-SP-8048.

COLE, M. O. T. ; KEOGH, P. S. ; BURROWS, C. R. Vibration Control of a Flexible Rotor/Magnetic Bearing System Subject to Direct Forcing and Base Motion Disturbance. Proc. Instn. Mech. Engrs. Vol.212 - Part C, 1998.

GÜLICH, J. F., "Centrifugal Pumps". 2nd Edition, Springer, Berlin, 2010.

KIM, C.-S. ; LEE, C.-W. Isotropic Optimal Control of Active Magnetic Bearing System. Transaction of the ASME, Journal of Dynamic Systems, Measurement, and Control. Vol. 118, pg.721-729. December 1996

OGATA, K. Engenharia de Controle Moderno. 2a. ed. Tradução de Ivan José de Albuquerque. Rio de Janeiro, Prentice-Hall do Brasil ltda, 1990.

ORSINI, L. Q. Introdução aos Sistemas Dinâmicos. Rio de Janeiro, Guanabara dois, 1985.

SUTTON, G.P. "History of Liquid Propellant Rocket Engines". American Institute of Aeronautics and Astronautics, Inc. 911 p. Virginia, USA. 2006.

YOUNCEF-TOUMI, K.; REDDY, S. Dynamic Analysis and Control of High Speed and High Precision Active Magnetic Bearings. Transaction of the ASME, Journal of Dynamic Systems, Measurement, and Control. Vol. 114, pg.623-633 December, 1992.

RESPONSIBILITY NOTICE

The author(s) is (are) the only party(ies) responsible for the printed material included in this paper.